Mechanical analysis and characterization of IGUs with different silicone sealed spacer connections - Part 1: experiments

Chiara Bedon · **Claudio Amadio**

Accepted: 16 May 2020

Abstract Due to several advantages, insulated glass units (IGUs) are largely used in buildings to realize curtain walls, vertical partitions but also roofs or pedestrian systems. The typical IGU consists of two glass layers, either monolithic and/or laminated sections, that can mechanically interact via an hermetically-sealed air (or gas) cavity between them. As known, load sharing phenomena have a crucial effect on the actual mechanical response of a given IGU. Accordingly, simplified analytical methods are available in the literature to account for these load sharing effects. The existing approaches, however, assume that the spacers providing the mechanical connection along the edges of glass panels are infinitely rigid. In this paper, original experimental tests are proposed for IGU specimens characterized by the presence of different types of spacer connections, as obtained from on a selection of configurations of technical interest. The actual mechanical contribution of spacer components is then investigated, giving evidence of major findings from small-scale shear and IGU four-point bending tests. Based on comparative test observations, the edge connection efficiency is then assessed for the investigated configurations.

Keywords Insulated glass units (IGUs) · Spacer connections · Load sharing effects · Experimental testing · Edge connection efficiency

C. Bedon (✉)· C. Amadio
Department of Engineering and Architecture, University of Trieste, Piazzale Europa 1, 34127 Trieste, Italy
e-mail: chiara.bedon@dia.units.it

1 Introduction

Insulated glass units (IGUs) are largely used in buildings, due to several advantages. From a pure mechanical point of view, the most relevant feature to account in the analysis of composite IGUs is that the actual load bearing performance is strictly related to the effects of combined (shared) loads, including also external (i.e., wind, crowd, maintenance, etc.) and internal (climatic effects due to environmental conditions) design actions requiring dedicated calculation methods. The structural role of linear spacer connections along the edges of glass panels (i.e., Fig. 1a), in this regard, represents a further aspect that still requires investigations. The number of influencing parameters for mechanical assessment purposes increases as far as the glass panels composing the IGU system are obtained via laminated glass (LG) sections, where the presence of a flexible interlayer foil with properties affected by time loading and temperature conditions should be properly taken into account (see for example Morse and Norville 2016; Bedon and Amadio 2018a, b; McMahon et al. 2018). As far as the presence of laminated panels and the mechanical interaction of glass layers (i.e., load sharing effects, see Sect. 2) is preliminary disregarded, the structural analysis of a given IGU should properly account for the contribution (stiffness and resistance) of the spacer components. A secondary seal (i.e., silicone, but also Polyurethane or Polysulfide, see Van Den Bergh et al. 2013) is commonly combined with a thin butyl layer

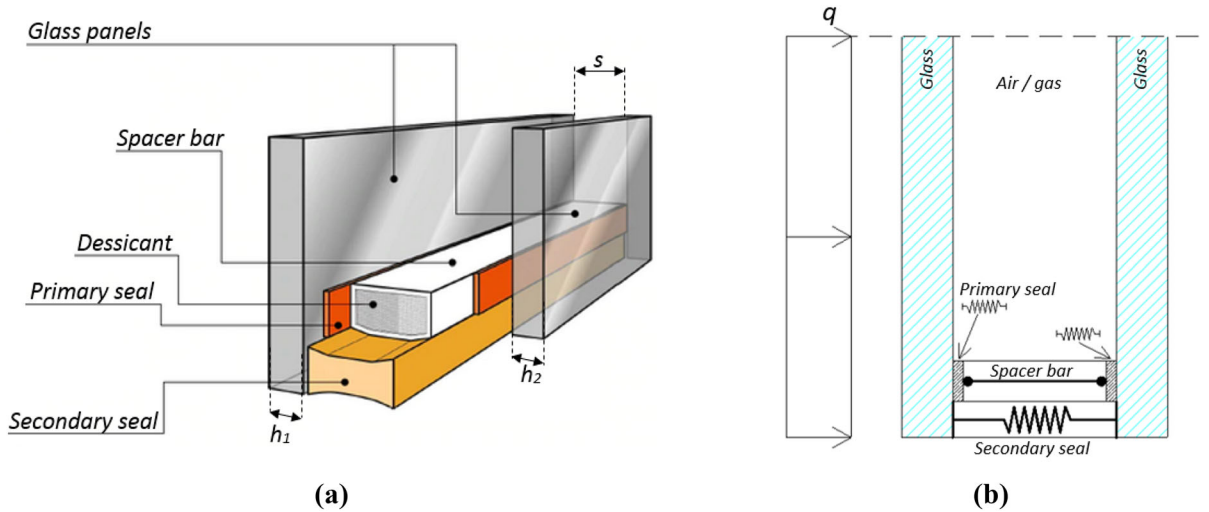

Fig. 1 Typical IGU composition and mechanical behaviour. **a** Key components (adapted from www.sika.com), with h_1, h_2 the thickness of glass panels and s the cavity. **b** Possible schematic mechanical model for the spacer connection under external design loads

and a mostly rigid spacer bar (consisting of a metal or fiberglass profile) to realize a continuous connection along the glass edges, see Fig. 1a.

The spacer bar is primarily intended to act as a "rigid support" in compression, so as to keep fix the distance of adjacent glass edges. A limited mechanical bond between the spacer bar and each glass panels is then offered by the primary seal (butyl), whose goal is to avoid vapour penetration and gas losses from the cavity. Besides its fundamental insulation role, the thermoplastic primary seal is generally fully disregarded as load-bearing component, and it is accepted to suffer for imposed stretches and compressive deformations, as required by the adjacent load-bearing members (see also Starman et al. 2020).

The secondary seal schematized in Fig. 1a, finally, has multiple roles in a given IGU. First, it protects the primary seal and gas cavity from vapour penetrations, but it also represents the mechanical component for the whole spacer connection. Its key requisites are thus a moderate stiffness and resistance in tension (to keep the glass panels together and avoid the edge separation), but also a certain flexibility (in order to accommodate the global movements and relative deformations of glass panels due to the imposed design loads). For ordinary design applications, extreme deformations induced by the secondary to the primary seals due to the mechanical interaction of adjacent bonds should be possibly minimized to avoid butyl corruption, see (Starman et al. 2020).

As such, the typical spacer connection can be regarded in the form of a partially flexible linear restraint with unilateral behaviour, whose schematic mechanical model is proposed in Fig. 1b. For the IGU under compressive pressures q distributed on the external glass surface, the spacer bar keeps fix the distance of the panels, while the sealant layers accommodate the required deformations (thus allowing a certain rotation at the panels ends due to global bending). Under tensile pressures, otherwise, the connection performance is strictly related to the effectiveness of the sealant layers only, given that the spacer bar cannot actively contribute to prevent the separation of glass edges.

In this research project, special care is spent for the assessment of the actual mechanical role of spacer connections in use for IGUs. Based on extended experimental analyses, the paper investigates the mechanical performance in shear and bending of IGU specimens characterized by different aspect ratios and spacer connection features. While secondary seals are realized with silicone strips, variations are accounted in the form of number of sealed edges, spacer bar features, etc. Relevant mechanical properties for these connections are thus derived from the experimental measurement, with a comparative discussion of test results.

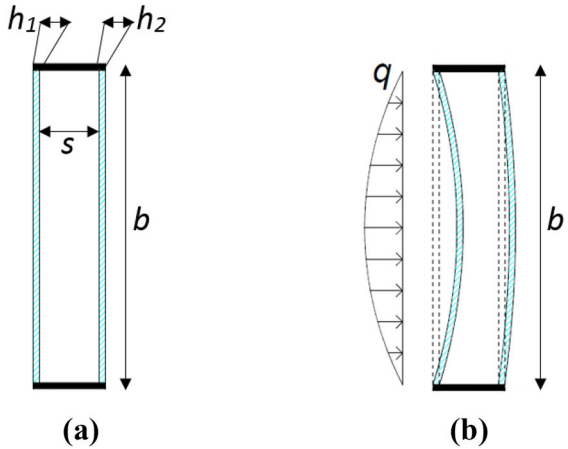

Fig. 2 Load sharing effects for **a** IGU systems due to **b** external pressures (prEN 13474-1)

To this aim, Sect. 2 first briefly recalls the basic assumptions of load sharing analytical formulations in use for IGUs, while Sect. 3 presents a description of test methods and materials. In Sects. 4 and 5, finally, a comparison of experimental outcomes is proposed, giving evidence of prevailing effects both in terms of failure mechanism and load-bearing performance for the tested IGUs. Successively ("Part II", see Bedon and Amadio 2020), the experimental results are further elaborated and investigated, with the support of analytical calculations and refined finite element (FE) numerical models able to account for a multitude of aspects, including the possible damage propagation of all the load-bearing components that are usually bonded in traditional IGUs.

2 Reference analytical models

2.1 Load sharing effects

In practice, IGUs are mostly composed of laminated glass panels able to offer enhanced thermal, acoustic and safety performances to these composite assemblies. The mutual interaction between these components, however, should be properly considered. In order to overcome major design difficulties, well-known simplified analytical models are available in the literature to account for load sharing effects in IGUs (Fig. 2).

Following the prEN 13474-1 provisions, a given external pressure q reflects in partial distribution among both the IGU layers (h_1 and h_2 their monolithic or equivalent thickness). The pressure amount on each glass panel is strictly related to the size and stiffness of each panel, as well as to the thickness s of the interposed cavity, see Table 1 and Fig. 3.

Table 1 Load sharing expressions for IGUs under a given external pressure q (prEN 13474-1)

Loaded panel	h_1	h_2
h_1 (outside)	$q_1 = (k_1 + \varphi\, k_2)\, q$	$q_2 = (1 - \varphi\,)\, k_2\, q$
h_2 (inside)	$q_1 = (1 - \varphi) k_1 q$	$q_2 = (\varphi k_1 + k_2)\, q$

Otherwise, the analytical method of Table 1 disregards the geometrical and mechanical properties of spacer connections in use. For a rectangular ($a \times b$) IGU with linear supports along the four edges it is in fact assumed that ($a \leq b$):

$$k_1 = \frac{h_1^3}{h_1^3+h_2^3} \tag{1}$$

$$k_2 = 1 - k_1 \tag{2}$$

and

$$\varphi = \frac{1}{1+\left(\frac{a}{a^*}\right)^4} \tag{3}$$

with

$$a^* = 28.9\sqrt[4]{\frac{h_1^3 h_2^3 s}{(h_1^3+h_2^3)k_5}} \tag{4}$$

the IGU characteristic length and k_5 is defined in the prEN 13474-1 document as a function of the aspect ratio $\lambda = a/b$, see Fig. 3a–c.

Based on Fig. 3d, moreover, it is possible to notice that the magnitude of load sharing effects is mostly affected by λ, and s-to-h ratios (in evidence, the load fraction that the panel "1" must carry on). The remaining part is transferred to the panel "2". Load sharing effects then progressively magnify for the panel "1" when the slenderness is relatively small ($\lambda < 0.4$). For larger λ values, otherwise, equal glass thicknesses $h_1 = h_2$ ideally carry on the same load magnitude. In (McMahon et al. 2018), it was experimentally proved for IGUs with $\lambda = 0.45$ that Fig. 3d is relatively close to the actual load sharing behaviour.

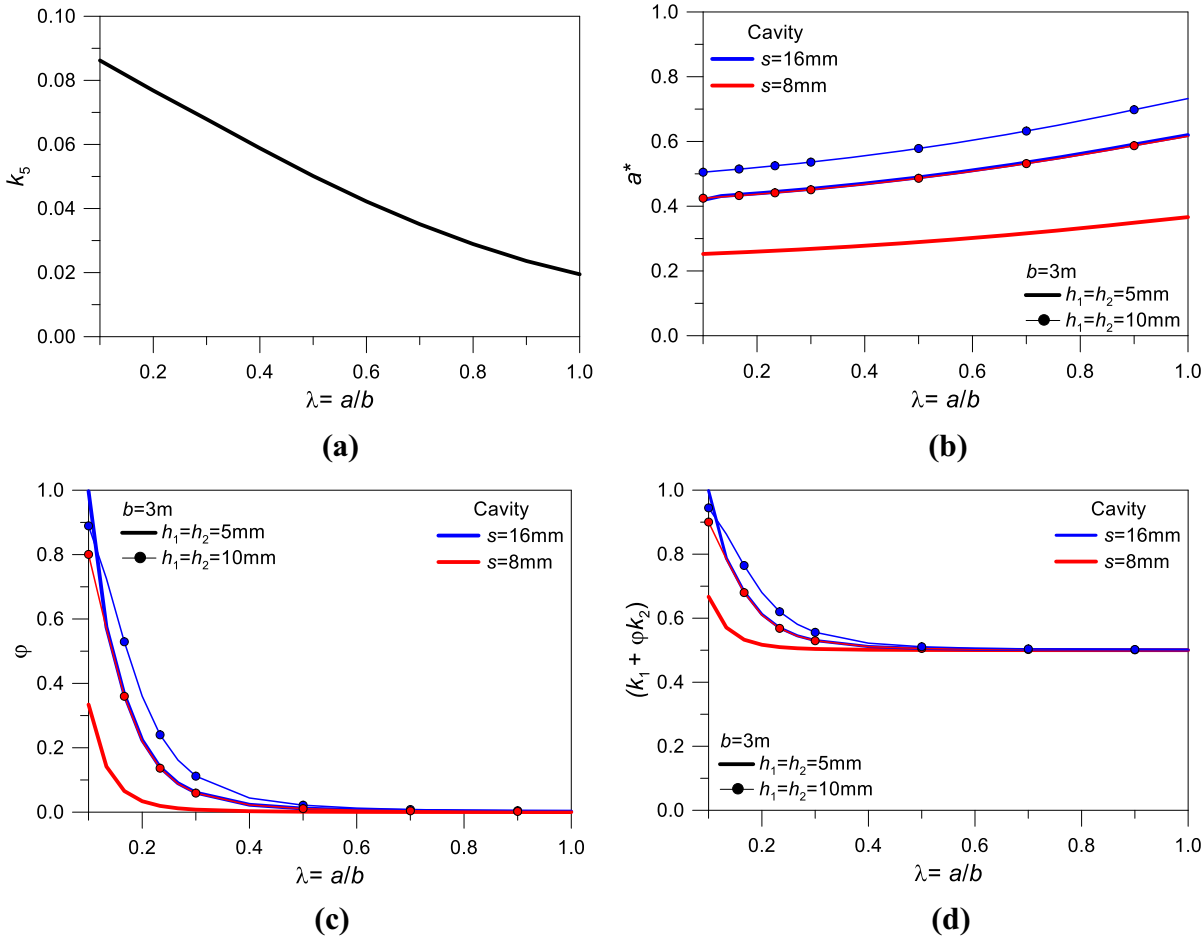

Fig. 3 Key parameters for load sharing calculations in IGUs (prEN 13474-1). In evidence, the typical variation of **a** k_5, **b** a^* and **c** φ coefficients as a function of the aspect ratio λ, with **d** load ratio for the glass panel under a given external pressure q

2.2 Adaptation of the γ-method for the assessment of spacer connection efficiency in IGUs

In this paper, a special focus is spent to experimentally assess the mechanical features and effects of typical spacer connections in use for IGUs. There, multiple components are in fact combined but (for design purposes) often disregarded.

From a mechanical point of view, the reference IGU schematized in Fig. 4 should be rationally regarded in the form of a composite (double glass) system whose structural response is strictly related to the presence of linear, flexible connections along the edges. As far as the connection features modify, the IGU bending performance is in fact expected to be comprised between the well-known limit conditions corresponding to the presence of:

- A rigid mechanical edge connection (and thus a fully monolithic behaviour for the glass panels, along their edges),
- Or a weak connection (being associated to a fully uncoupled behaviour of glass panels).

Consequently, an accurate estimation of connection features and effects for IGUs still represents an open question. Such a design issue is in close correlation with a multitude of structural typologies involving the bonding of multiple load-bearing elements via partially rigid connections (both continuous or lumped), and several simplified approaches are available in the literature. Among others, the Eurocode 5 for timber structures (EN 1995-1-1) suggests for composite beams with

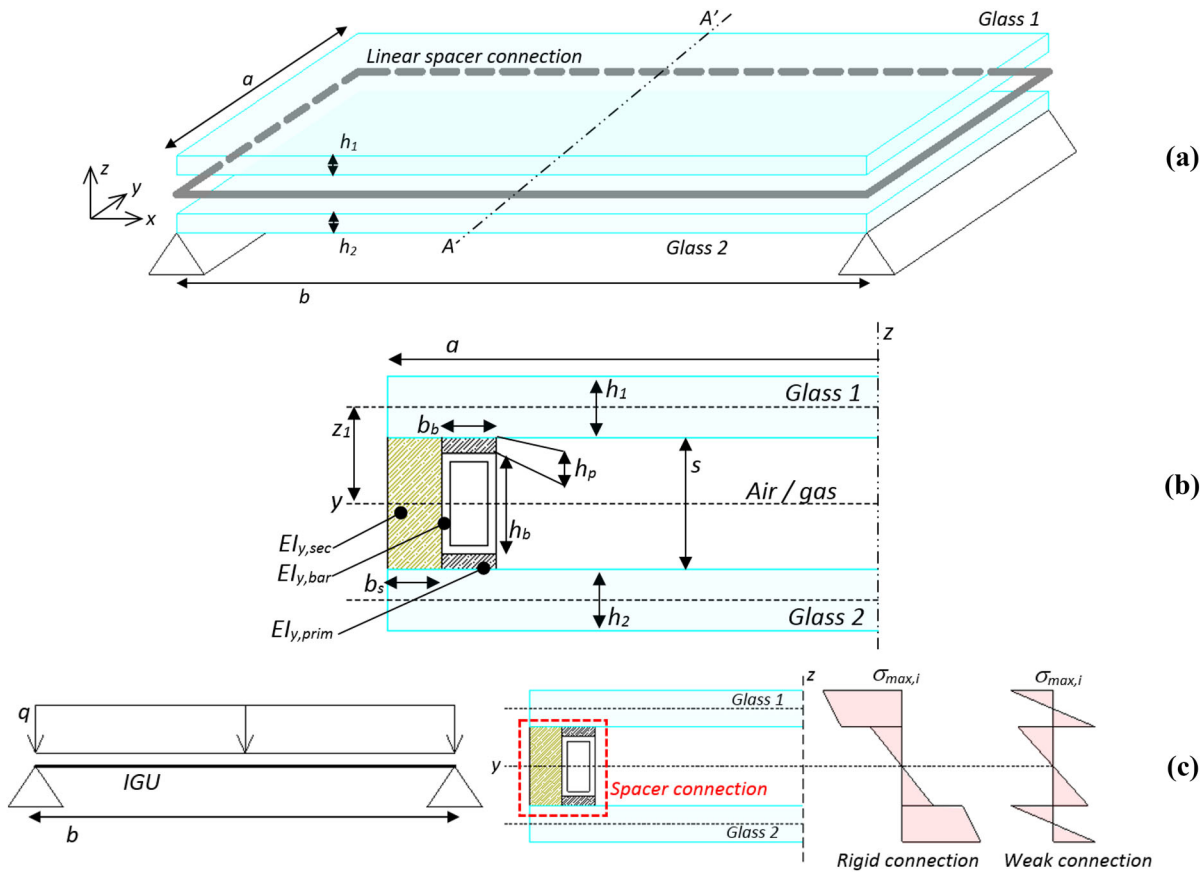

Fig. 4 Bending performance of double symmetric IGUs with 4-sealed edges: **a** reference model and **b** A-A′ cross-section (edge detail), with **c** expected stress distribution, as a function of the connection efficiency

flexible connection the use of the well-known Möhler (or γ-) method (see Möhler 1956). The latter refers to simply supported beams in bending, but can be easily extended and adapted to 4-edge sealed IGUs with a prevailing beam-like behaviour. This is the case of various applications for roof or wall IGUs, with 2-side linearly restrained edges (see for example Bedon and Amadio 2018b).

More in detail, the effective bending stiffness of the double symmetric IGU in Fig. 4a can be rationally calculated as:

$$(EI)_{y,eff} = \sum_{i=1}^{2} E_g I_{y,i} + \gamma \cdot \left(2 E_g A_i \cdot z_i^2\right) + n_b \cdot \left(2 E I_{y,bar}\right) + n_s \cdot \left(2 E I_{y,sec}\right) \quad (5)$$

where

- E_g represents the modulus of elasticity (MoE) of glass;
- $A_i = A = a \times h_i$ is the cross-section of each glass layer ($i = 1, 2$);
- $I_{y,i} = (a \times h_i^3)/12$ is the corresponding second moment of area ($i = 1, 2$);
- z_i ($i = 1, 2$) represents the distance between the middle axis of each glass panel and the middle longitudinal axis for the IGU as a whole.

For a given transversal cross-section that includes two spacer connections (i.e., the A-A′ section in Fig. 4a), Eq. (5) takes into account the glass components listed above and two additional contributions, namely represented by the box spacer bars ($b_b \times h_b$ their outer section size) and the silicone layers ($b_s \times s$ the cross-section). Both these components are considered in the longitudinal direction only (i.e., where they are expected to bend about their major axis), while the a-long spacer connections in Fig. 4a are expected to be minimally

involved in the global bending resisting mechanism for the IGU.

The contribution of spacer bars ($EI_{y,bar}$ in Fig. 4b) is estimated based on the homogenization factor $n_b = E_{bar}/E_g$, with E_b the MoE for the box section (aluminium, or other materials) and $I_{y,bar}$ the second moment of area. Each silicone joint, given the size and mechanical properties, can only slightly improve the so-calculated global bending stiffness, with $n_s = E_s/E_g$ in Eq. (5) and E_s the MoE for the adhesive in use. Finally, Eq. (5) disregards the effect of primary seal layers (with $b_b \times h_p$ their nominal dimensions, and $EI_{y,prim} \approx 0$ their bending stiffness).

The connection efficiency γ in Eq. (5) is commonly comprised between $\gamma = 0$ (weak connection) and $\gamma = 1$ (rigid bond). As far as γ modifies as a function of the connection features, the IGU bending resisting mechanism is expected to manifest in different stress distributions for the glass panels (Fig. 4c). The edge connection features are also directly responsible of the ultimate load-bearing capacity of the IGU in Fig. 4. Assuming that stress peaks in glass do not exceed the tensile strength and behave linear elastically for a given external load q (thus bending moment $M_{y,max}$ and shear V_{max}), the longitudinal relative sliding of glass panels is prevented by the linear spacer connections only.

Various literature studies applied the direct Möhler method to calculate reliable γ-values for different structural typologies, based on the geometrical and mechanical features of load-bearing components, and also for structural glass systems (see also Feldmann et al. 2010, 2014; Firmo et al. 2016). In this paper, an inverse calculation approach is used for γ-estimates, based on Eq. (5) and on the experimental analysis of IGUs in bending. As a result, γ is calculated so as to capture the $(EI)_{y,eff}$ stiffness corresponding to the experimentally measured load-deflection estimates.

2.3 Sandwich theory for spacer connection efficiency in IGUs

As a further validation of the connection efficiency for IGU details according to Fig. 4, the sandwich beam-based analytical model proposed in Pascual et al. (2019) is taken into account and further explored in "Part II" (Bedon and Amadio 2020). The latter—with geometrical variations to account for details in Fig. 4 – well applies to the reference mechanical systems herein explored. In accordance with Fig. 5, the mid-span deflection can be calculated for the equivalent static scheme in Fig. 5a, where:

$$w = w_A = -\left(w_{global,B} + w_{local,B} + w_{global,C} + w_{local,C}\right) \tag{6}$$

Among others, key parameters for the bending performance assessment in Fig. 5b are the local (D_{local}) and global (D_{global}) rigidity contributions, that for the IGU in Fig. 4 can be rationally adapted in:

$$D_{local} = \sum_i E_i \int_{A_i} z_{local_i}^2 \, dA_i = (D_{local})_{top\ glass} + (D_{local})_{bottom\ glass} + (D_{local})_{spacer\ connections} \tag{7}$$

and

$$D_{global} = \sum_i E_i \int_{A_i} z_{global_i}^2 \, dA_i = \left(D_{global}\right)_{top\ glass} + \left(D_{global}\right)_{bottom\ glass} + \left(D_{global}\right)_{spacer\ connections} \tag{8}$$

Another relevant parameter is then represented by the cross-sectional shear stiffness:

$$U = G_{joint}\, A_{shear,sandwich} \tag{9}$$

that directly involves the shear stiffness of sealants in use, and the joint properties. Assuming that the mechanical features of the IGU spacer connections are ideally comprised between the *layered* and *monolithic* conditions, moreover, the efficiency parameter is estimated as:

$$\eta = \frac{w_{layered} - w}{w_{layered} - w_{monolithic}} 100\% \tag{10}$$

3 Experimental investigation: materials and components

A series of laboratory tests was carried out at the Department of Engineering and Architecture, University of Trieste (Italy). All the quasi-static, short-term destructive experiments were carried out in winter, in non-controlled laboratory conditions, with 8 °C the mean temperature and 80% the Relative Humidity.

In accordance with the schematic representation of Figs. 1 and 4, the investigation was focused on IGU

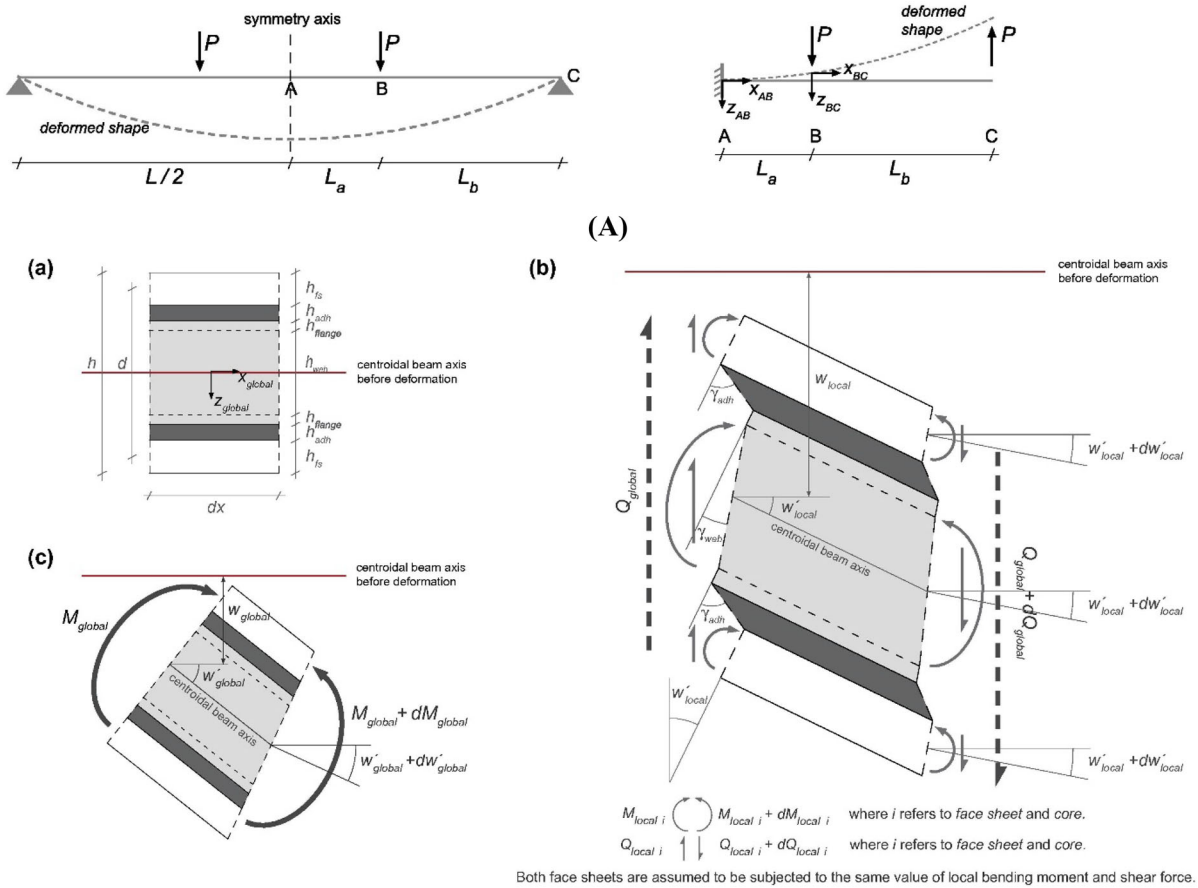

Fig. 5 Sandwich-beam based analytical model from Pascual et al. (2019): **A** reference equivalent scheme for a four-point bending loading scheme and **B** global bending response scheme (figures reproduced from Pascual et al. (2019) with permission from Elsevier—Copyright © license number 4795891403469, March 2020)

specimens composed of two monolithic annealed (AN) glass panels, with a fix cavity thickness $s = 16$mm. Throughout the experimental study, key variations were represented by the composition and features of spacer connections in use to bond the glass edges (Sects. 3.1–3.3). Differing from common practice, the choice of AN monolithic panels was privileged at the time of the experimental project, to better assess the mechanical characteristics of spacer connections, thus avoiding additional influencing parameters due to the presence of possible interlayers. The additional advantage due to the use of AN panels was to disregard possible residual effects that are typical of pre-stressed glass, being out of the scope of this research study. According to product standards, AN elements are characterized by a mean modulus of elasticity $E_g = 70$GPa, with $f_{tk} = 45$MPa the mean tensile bending resistance (characteristic nominal value) and $\nu_g = 0.23$ the Poisson' ratio, while the material density is $\rho_g = 2500$kg/m^3 (EN 572-2).

3.1 Spacer bars

Two different spacer bars were used for the tested specimens. A first group of experiments was carried out by taking into account the traditional Aluminium (AL) spacer H65 ®, profile A155, from AluPro (www.alupro.it). The bar is composed of an AL alloy (EN-AW-3005 type, temper H26). According to EN 573-3 and EN485-2 product standards, this alloy offers a mean $E_{al} = 70$GPa, with $\rho_{al} = 2721$kg/m^3. Min-

Table 2 Nominal dimensions for the selected aluminium (AL) and Warm Edge (WE) spacer bars

AL spacer bar Aluminum spacer H65® – Profile A155 (AluPro)		WE spacer bar CHROMATECH Ultra® 16 – Version F (AluPro)	
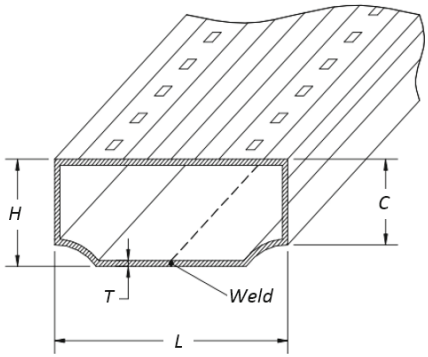		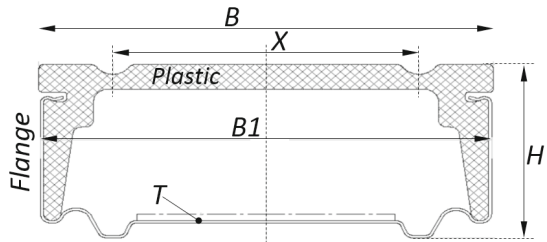	
L (mm)	15.50 (± 0.1)	H (mm)	6.9 (± 0.15)
H (mm)	6.50 (± 0.1)	Flange (mm)	5.1 (± 0.1)
C (mm)	5.10 (± 0.2)	B (mm)	15.6 (± 0.15)
T (mm)	0.31 (± 0.01)	B1 (mm)	15.5 (± 0.15)
		X (mm)	10.45 (± 0.1)
		T (mm)	0.1

imum nominal values of tensile strength at yielding and ultimate conditions are $f_{y,al} = 160$Mpa and $f_{u,al} = 195$MPa (minimum), with $\varepsilon_{u,al} = 9\%$ the nominal elongation at failure. Reference dimensions for the typical cross-section in use for the experimental investigation can be found in Table 2.

For comparative purposes, a novel Warm Edge (WE) spacer was also considered for some of the tested IGU specimens. The typical profile, see Table 2, consisted in the CHROMATECH Ultra®16 by AluPro—Version F, as proposed for IGUs with $s = 16$mm thick cavities. Its resisting cross-section is obtained by a stainless steel profile [AISI 201 type (EN.14372 alloy according to EN 10088-2: 2014 provisions)] and a top plastic flange [Polycarbonate (PC)]. For the steel section, nominal mechanical properties are assumed in $E_{st} = 197$GPa, with $f_{y,st} = 360$MPa and $f_{u,st} = 750$MPa (EN 10088-2: 2014), while for the PC flange $E_{pc} = 2.6$GPa and $f_{y,pc} = f_{u,pc} = 60$MPa.

3.2 Primary seal

As usual, the mechanical interaction of spacer bars with the adjacent glass panels is ensured by the presence of primary and secondary sealants. Only the seconds, however, are specifically intended for load-bearing applications. Throughout the parametric experimental analysis herein discussed, the primary seal for all the tested specimens consisted in a layer of Butylver® sealant [Fenzi (www.fenzigroup.com)].

Given the cavity gap $s = 16$mm, the use of spacer bars according to Table 2 resulted in a mean thickness for Butylver®in the order of $h_p = 0.25$mm. Butylver is a one-part polyisobutylene (PIB)-based material, totally solvent free, especially formulated for use as primary seal in insulated units. Key nominal properties of this thermoplastic sealant are low density ($\rho_p = 1.09$ gr/cm^3 at 20 °C), minimum water vapor transmission rate (< 0.1 gr/m^3 d) and high gas permeation rate (< 0.002 gr/m^2 h), see www.fenzigroup.com. Otherwise, PIB mechanical properties are characterized by relatively low stiffness and tensile/shear resistance. As far as the imposed deformations are limited in magnitude, reversible deformations of primary seals do not affect the cavity (and thus IGU) conditions. Critical issues can otherwise derive from changes in material properties or temperature/loading cycles, and thus possible permanent deformations that could compromise the integrity/insulation of the unit (Starman et al. 2020). Experimental studies of literature report

Table 3 Summary of experimental tests on IGU components and small-scale specimens

Test type	Specimen type	No. of specimens
Shear	IGU joint	2
Four-point bending	Small-scale IGU panel	25

mean values of MoE and tensile strength in the order of $E_p = 0.56$MPa and $f_{u,p} = 0.25$MPa respectively, see for example (Turowec and Gillies 2016). Among others, as a thermoplastic material, a certain sensitivity of thermo-mechanical properties to operational conditions can be rationally expected, and should be further taken into account for load-bearing performance assessment if IGUs (see for example Nguyen-Tri et al. 2019).

3.3 Secondary seal

Regarding the secondary seal, the DOWSIL^{TM} 3363, two-part silicone sealant by Dow Corning was used (www.dow.com). According to technical data sheets, the nominal longitudinal MoE is expected in $E_s = 4.8$MPa, with $f_{u,s} = 1.5$MPa the tensile resistance (www.dow.com). In accordance with the schematic cross-section of Fig. 4, silicone joints with both $b_s = 6$mm or $b_s = 9$mm nominal width were taken into account for the tested specimens.

3.4 Number of specimens

The experimental program included preliminary shear tests on small-scale IGU joints, followed by a series of bending tests on IGU prototypes. All these destructive tests were performed in laboratory conditions on a total of 27 specimens (Table 3). A more detailed description of mechanical and geometrical features for all the specimens, as well as test setup and experimental methods, is provided in Sects. 4–5.

4 Shear experiments on IGU joints

4.1 Methods

Two IGU joint specimens inclusive of typical spacer connections were first investigated. Each sample, for convenience, was assembled in the form of a triplet shear test setup (Fig. 6), and consisted of three AN monolithic glass plates ($a = 200 \times b = 200$mm their nominal size) with $h = 5$mm their thickness.

The joint specimen included four linearly sealed edges, composed each one of a WE spacer bar (Table 2), primary seal joints (with $h_p = 0.25$mm the average thickness) and secondary silicone layers (with $b_s = 6$mm their width). Given that the middle glass panel ("Glass 2", in Fig. 4a) was shifted $\Delta b = 20$mm compared to the external plates ("Glass 1" and "Glass 3" in Fig. 6a), the final specimen was characterized by the presence of $L = 180$mm long bonded regions. Two specimens (#1 and #2) with identical nominal geometry and spacer connections were taken into account, to collect preliminary considerations.

The reference setup, see Fig. 6, was organized so that each IGU joint could be fixed at the base of the external panels ("1" and "3"), while introducing pure shear loads (in the same direction of sealed edges) on the middle layer ("2"). Three C-shaped steel profiles were used to position the specimens in the testing machine, as well as to distribute the imposed load along the width $a = 200$mm. The goal was to capture the shear resisting behaviour of the spacer connections in use (in this case, a WE bar with primary and secondary seals). Under the action of in-plane shear loads, the spacer bar was in fact expected to undergo rigid-body translations, with a mostly null contribution to the overall mechanical behaviour of the joint. Accordingly, shear stiffness and resistance contributions were obtained from the primary and secondary seals. However, it is also recognized that WE or AL bar details (material, profile, surface, etc.) could affect the adhesion of sealant layers in use, thus their ultimate load-bearing performance. Additional influencing parameters to take into account would be certainly represented by operational conditions (ambient, loading rate), thus suggesting the need of extended parametric experimental analyses.

In order to monitor the whole shear performance of the edge connections, two Linear Variable Displacement Transducers (LVDTs) were used to monitor the deformation of panel "2" (one LVDT on each face), while increasing the imposed quasi-static shear load. The corresponding displacements were recorded with a sampling frequency of 10Hz. The typical test duration was in the range of 16–18 min. The imposed load was first monotonically increased up to a first peak of ≈ 2.5kN (with a loading rate of 1mm/min). Each spec-

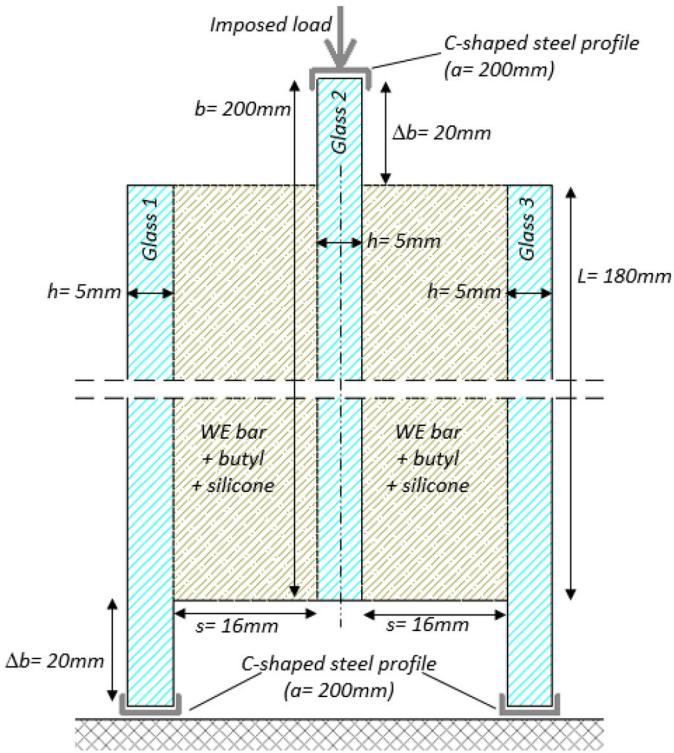

(a)

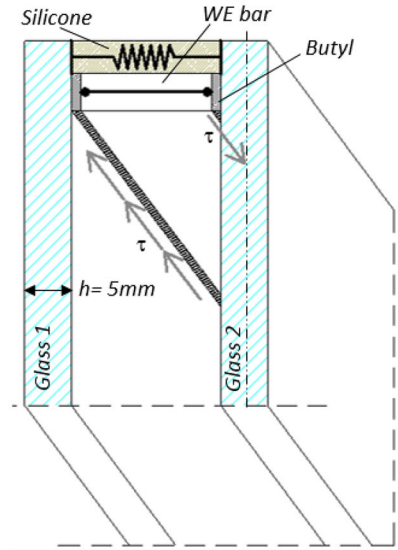

(b)

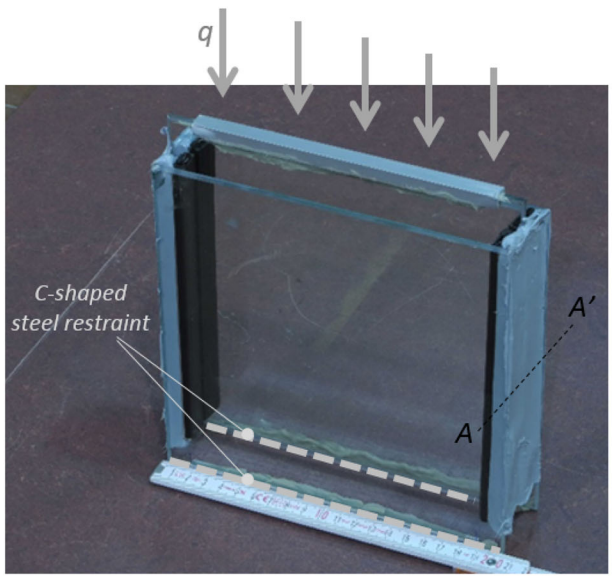

(c)

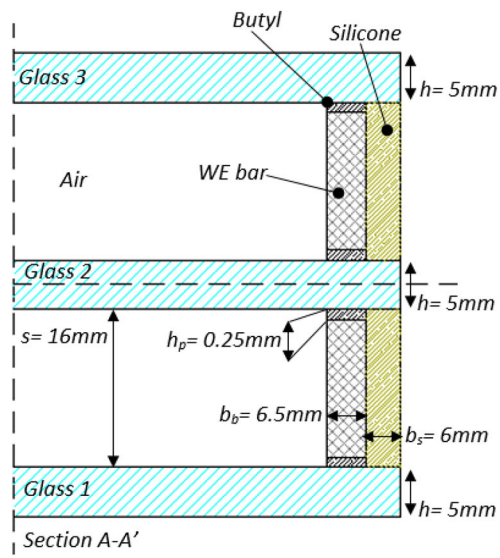

(d)

Fig. 6 Small-scale IGU joint specimen: **a** lateral view and **b** expected shear resisting mechanism; with **c** specimen axonometry and **d** schematic transversal cross-section

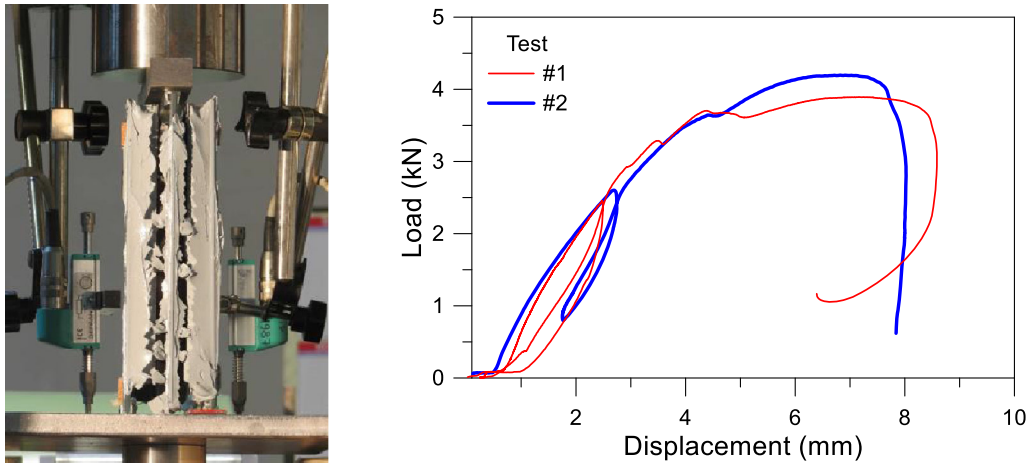

Fig. 7 Shear tests on IGU joints: **a** typical failure scenario and **b** load-displacement results

imen was then fully unloaded and reloaded up to collapse (1.5 mm/min).

4.2 Results

Even in presence of a limited number of test repetitions, the specimens gave evidence of a relatively stable and ductile behaviour in shear. Figure 7a shows the typical shear resisting mechanism and failure response that was experimentally observed for the two samples (#1 and #2). The latter occurred due to the progressive damage propagation at the interface between the continuous spacer connections (sealing bonds) and the glass panels, up to the final separation of the involved glass components.

The IGU joints proved to resist up to a mean shear load $F_{\text{shear}} = 4.05\,\text{kN}$ ($\pm 0.21\text{kN}$ the standard deviation), see Fig. 7b. For both the specimens, the typical failure mechanism was observed at an average imposed deformation of $\delta_{\text{u}} \approx 8\text{mm}$.

Given that each IGU triplet specimen consisted of $n_{\text{edges}} = 4$ sealed edges, with $n_{\text{bond}} = 8$ bonded regions in total, the maximum resistance for the typical "butyl + silicone" joint was calculated by taking into account the symmetry of the test setup in use, that is:

$$F_{joint} = \frac{F_{shear}}{n_{edges}} = 1.0125\,\text{kN} \tag{11}$$

Otherwise, the load-bearing response of joint details according to Fig. 6d mainly depends on the silicone layers (due to the limited resistance of butyl components). Assuming that each edge was bonded over a $b_{\text{s}} = 6\,\text{mm} \times L = 180\,\text{mm}$ shear resisting surface (corresponding to a single silicone joint), it is:

$$A_{bond} = b_{\text{s}} L = 1080\,\text{mm}^2 \tag{12}$$

thus

$$\tau_{joint} = \frac{F_{shear}}{n_{bond}} \cdot \frac{1}{A_{bond}} = 1.84\,\text{MPa} \tag{13}$$

represents the mean experimental value of the ultimate shear strength.

Besides Eq. (13) fully disregard the possible contribution of Butylver joints (with $\approx 0.25\text{MPa}$ the expected ultimate reference value in tension, Sect. 3.2), the calculated value suggests the fundamental role of sealants in use for load-bearing purposes in similar joints, as well as the need of dedicated characterization studies. The so calculated shear stress τ_{joint} is in fact rather in correlation with the nominal resistance of silicone joints ($\approx$ 1.5 MPa, Sect. 3.3, that is $+22.7\%$). At the same time, moreover, it is worth of interest to remind that the actual mechanical properties and performances of the seals in use are typically sensitive to strain rate and ambient temperatures. Additional uncertainties may derive then from the production stage.

Further efforts were thus carried out, based on Fig. 7b, to characterize the resisting mechanism of each edge connection, with respect to stiffness parameters of interest for design. The ultimate (K_u) and serviceability (K_{ser}) shear stiffness values, in particular, were calculated for each IGU specimen as:

$$K_u = \frac{0.6\,F_{shear}}{\frac{6}{5}\,(\delta_{06} - \delta_{01})} \approx 1.234\,\text{kN/mm} \tag{14}$$

and

$$K_{ser} = \frac{0.4\,F_{shear}}{\frac{4}{3}\,(\delta_{04} - \delta_{01})} \approx 1.168\,\text{kN/mm} \tag{15}$$

respectively, with δ_{06}, δ_{04} and δ_{01} the measured average sliding amplitudes (in Fig. 7b) corresponding to the 60%, 40% and 10% part of the experimental failure load.

Accordingly, stiffness estimates for a typical IGU connection (i.e., a single edge connection over the 4 in use for each specimen) were defined as:

$$K_{u,joint} = \frac{K_u}{n_{edges}} \approx 0.3085\,\text{kN/mm} \tag{16}$$

$$K_{ser,joint} = \frac{K_{ser}}{n_{edges}} \approx 0.292\,\text{kN/mm} \tag{17}$$

Again, given that the shear flexibility of each spacer connection can be reasonably expected to mostly derive from the shear deformation of silicone layers, a final attempt was carried out to predict the equivalent, secant stiffness of a single silicone strip, that is:

$$G_{joint} = \frac{s \cdot K_{ser,joint}}{2 \cdot A_{bond}} = 2.16\,\text{MPa} \tag{18}$$

$$E_{joint} = G_{joint}\,(2 \cdot (1 + \nu_s)) \approx 6.44\,\text{MPa} \tag{19}$$

with $\nu_s = 0.49$. As shown, Eq. (19) overestimates the expected nominal MoE for the silicone layers in use (with $E_s = 4.8$ MPa, see Sect. 3.3, that is $+34.2\%$). The latter could be further explained in terms of operational conditions (low laboratory temperature), possible interaction with the butyl layers (especially in the preliminary elastic stage), as well as a possible stiffening effect due to the lateral confinement effect due to spacer bars in use.

Otherwise, the so estimated material properties directly reflects on the connection efficiency parameters previously recalled in Sect. 2. As such, a future experimental investigation should possibly account for a multitude of operational configurations of technical interest for IGUs under ordinary/extreme design loads and ambient conditions.

5 Bending tests on IGU specimens

5.1 Methods

IGU prototypes were tested under a four-point bending setup. The specimens were designed with:

- $a = 400\text{mm} \times b = 1100\text{mm}$, that is $\lambda = 0.36$ (group I, Table 4), and
- $a = 300\text{mm} \times b = 1100\text{mm}$, $\lambda = 0.27$ (group II, Table 5).

Among the two series, the difference was given by the thickness of glass ($h_1 = h_2$) and by the connection detailing, including variations in:

- Type of spacer bar (AL or WE);
- Number of sealed edges for a given IGU (2 or 4 sealed edges);
- Presence (or not) of primary (butyl) seal;
- Presence (or not) of secondary (silicone) seal;
- Number of sealed edges with secondary seal;
- Thickness of secondary layer (with $b_s = 6\text{mm}$ or 9mm)

In Tables 4, 5, a list of properties is presented for all the tested specimens. Labels of test series are given in the form so that the number of sealed edges and the type of components can be easily detected, where:

"number of edges with spacer bar" (2C or 4C) "number of edges with silicone layer" (2S or 4S, if any) "_WE (spacer bar)" (suffix removed for AL bars)

For each test series, finally, each specimen with given geometrical and mechanical properties is detected by the suffix "*_number*" (with *number* ≥ 1).

Careful consideration was spent for the assessment of mechanical features of the spacer connections in use. Accordingly, the experimental study was divided into two groups:

- First (group I), IGU specimens with two sealed edges only were taken into account (longest edges, with unsealed short edges). Given the lack of hermetically sealed cavity between the glass panels, these specimens were investigated in order to avoid load sharing effects and specifically focus on the stiffness contribution of spacer components. A single test repetition was carried out on 2-edge sealed specimens with a typical beam behaviour, while the attention was focused on the role of primary and secondary seals (Table 4).
- Successively (group II), further IGU specimens were investigated under the same bending test setup. In this latter case, however, all the four edges were properly sealed, and the interposed cavity was filled with air (1 atm the internal pressure). The secondary silicone seal was progressively introduced in the samples, and also fully omitted for some of them (Table 5).

Quasi-static bending experiments were carried out in accordance with the test setup proposed in Fig. 8. In analogy with the shear setup in Sect. 3, the loading rate was set in 1mm/min for a first cycle, then increased to 1.5 mm/min for the reloading stage, up to collapse.

In general, the bending setup for the IGU samples in simply supported condition was defined so that the vertical loads could be applied to the top glass panel. In this manner, the composite action of each IGU sample was made possible by activation of the linear edge connections.

Two cylindrical steel devices were used to reproduce the simply supported configuration of IGU specimens (Fig. 8a, b). At the same time, the vertical loads were introduced through a set of three steel members (two flat steel plates and one transversal UPN profile), so as to distribute them on the whole width a of each specimen (Fig. 8a, c). Two rubber strips were interposed between steel and glass, in order to avoid potential local contact damage.

To this aim, the experimental instruments were properly installed so as to capture the global and local bending response of IGU specimens. A total of 10 LVDTs was used to monitor the key deformation of each sample, see Figs. 8c and 9.

Among the 10 LVDT instruments in use (Figs. 8d, 9a), some of them were used to monitor the bending deformations of the tested IGU specimens, with:

- P#4 and P#7 at midspan,
- P#3 and P#6 at the left support,
- P#5 and P#8 at the right support.

Few others, see the P#9 and P#10 (detailed view in Fig. 9b) were installed to monitor the relative sliding of glass panels in the longitudinal direction, being each tested IGUs in bending expected to work as a composite system with partially flexible connection along the edges. Finally, P#11 and P#12 instruments were used to assess any possible scatter in the vertical deformations (thus uplift or compression, due to local deformations of the bonding layers) of the top and bottom glass panels.

5.2 Analysis of results

Major experimental efforts were spent, in the post-processing stage, for the analysis of the bending performances of IGUs with different features. Among the different typologies of spacer components in use (Tables 4, 5), the analysis was first aimed at a possible quantification of the mechanical effects due to primary or secondary seals. Another relevant parameter of the experimental study was then represented—for fixed global dimensions and spacer type—by the glass-to-spacer stiffness ratio. The analysis of test results was hence focused on:

- Failure mechanism and crack pattern evolution for the tested specimens,
- Load-deflection,
- Load-relative slip,
- Effective bending stiffness (at collapse or at intermediate load levels).
- *Failure mechanism*

Table 4 Four-point bending tests (group I, with $a = 400\,\text{mm} \times b = 1100\,\text{mm}$). Key: AL = aluminum; WE = Warm Edge; P = primary seal (Butylver 0.25 mm); S = secondary seal (silicone DOWSIL 3363); Y = yes; X = no

Series	Test repetitions	Label	h_1, h_2 (mm)	Spacer bar	Seal type	Sealed edges in total	Secondary seal (n. of sealed edges), b_s (mm)
2C	1	2C_01	5	AL	P	2	X
2C_WE	1	2C_WE01	5	WE	P	2	X
2C2S	1	2C2S_01	5	AL	P + S	2	Y (2), 9
2C2S_WE	1	2C2S_WE01	5	WE	P + S	2	Y (2), 9
Total	4						

A qualitative comparison of collected test results was first carried out in terms of failure mechanism for the tested IGUs. A careful attention was paid for the visual detection of first macro cracks in both the glass panels (position and fracture pattern), as observed during the imposed bending deformations. Generally, a linear elastic behaviour with brittle collapse mechanism was observed for the tested samples. In Fig. 10, for example, the deflection (mid-span section, as obtained from the average of P#4 and P#7 records) is proposed for selected 2-edge sealed specimens (5 mm thick panels) or 4-edge sealed specimens respectively (10 mm thick panels with primary seal and AL bar), as a function of the total imposed load.

For all the specimens, the governing failure mechanism leading the experiments to conclusion was mostly characterized by the propagation of cracks in the bottom glass panel (due to the achievement of maximum tensile stress peaks, according to the test setup in use). These first glass cracks were found to compromise the whole bending performance of the specimens, with null residual resistance and ductility. All the cracks originated from one of the longest edges of the panels, and then propagated in the full width of the specimens.

Basically, the distinction of experimental outcomes was thus made in terms of (1) crack pattern/distribution and (2) origin of cracks, given that all the specimens typically reflected two phenomena:

(a) Several simultaneous cracks, or
(b) A single severe crack (with origin close to the IGU mid-span section, or in the region of load introduction), with radial pattern,

or eventually:

(c) A mixed cracking mechanism [combination of (a) and (b)].

In Fig. 11 and Tables 6, 7 and 8, some comparisons are thus proposed for groups of specimens (listed by $a \times b$ dimensions, or glass thickness, or spacer bar type).

Based on the collected test observations, in particular, it was shown that:

- For the specimens with 2-edge spacer connections ("2C" specimens, see Table 6) the failure mechanism was typically associated to a combination of multiple, independent cracks in glass. For one specimen only (see "2C2S_WE01" in Table 6), collapse was associated to a single radial crack (see Fig. 11c, d). Besides the limited number of experiments/test repetitions, from Table 6 it is also interesting to notice that the specimens inclusive of silicone joints ("2C2S" type) where characterized by cracks propagating from the loading region (in place of mid-span section). Such a behaviour could be associated to the presence (with silicone joints) of an additional flexibility along the edges of glass;

while the 4-edge sealed specimens (10 mm thick panels) showed that:

- In the case of IGUs with AL spacer bar (Table 7), the prevailing failure mechanism was governed by a single radial crack propagating from the edge of the bottom glass panel (region of load introduction). The crack origin moved to mid-span section for few specimens only, mostly without silicone joints;
- For the specimens with WE spacer bar (see Table 8), a mostly scattered performance was observed. Given that the bending response was in any case a linear elastic one with brittle collapse, for most of the specimens in Table 8 multiple cracks simultaneously propagated from the bottom and top panels (see the "n.a." cases in Table 8). No prevailing crack patterns were defined, with mixed crack distributions and locations.

Table 5 Four-point bending tests (group II, with $a = 300\,\text{mm} \times b = 1100\,\text{mm}$). Key: AL = aluminum; WE = Warm Edge; P = primary seal (Butylver 0.25 mm); S = secondary seal (silicone DOWSIL 3363); Y = yes; X = no. * = specimens with $a = 400\text{mm} \times b = 1100\text{mm}$

Series	Test repetitions	Label	h_1, h_2 (mm)	Spacer bar	Seal type	Sealed edges in total	Secondary seal (n. of sealed edges), b_s (mm)
4C	3	4C_01	10	AL	P	4	X
		4C_02	10	AL	P	4	X
		4C_03	10	AL	P	4	X
4C_WE	3	4C_WE01	10	WE	P	4	X
		4C_WE02	10	WE	P	4	X
		4C_WE03	10	WE	P	4	X
4C2S	3	4C2S_01	10	AL	P + S	4	Y (2), 6
		4C2S_02	10	AL	P + S	4	Y (2), 6
		4C2S_03	10	AL	P + S	4	Y (2), 6
4C2S_WE	3	4C2S_WE01	10	WE	P + S	4	Y (2), 6
		4C2S_WE02	10	WE	P + S	4	Y (2), 6
		4C2S_WE03	10	WE	P + S	4	Y (2), 6
4C4S_AL	3	4C4S_AL01	10	AL	P + S	4	Y (4), 6
		4C4S_AL02	10	AL	P + S	4	Y (4), 6
		4C4S_AL03	10	AL	P + S	4	Y (4), 6
4C4S_WE	3	4C4S_WE01	10	WE	P + S	4	Y (4), 6
		4C4S_WE02	10	WE	P + S	4	Y (4), 6
		4C4S_WE03	10	WE	P + S	4	Y (4), 6
4C4S_WE*	3	4C4S_WE01	5	WE	P + S	4	Y (4), 9
		4C4S_WE02	5	WE	P + S	4	Y (4), 9
		4C4S_WE03	5	WE	P + S	4	Y (4), 9
Total	21						

In the same tables, γ-values are also presented for each specimen, as obtained based on the test setup of Fig. 8 and the bending experimental measurements in Sect. 5.3. Given that the mid-span deflection for the tested IGUs is given by:

$$f_{\max} = \frac{F_{tot} d \cdot \left(3(b-2d)^2 - 4d^2\right)}{24\,(EI)_{y,eff}} \tag{20}$$

the equivalent stiffness in Eq. (5) was first calculated based on the nominal geometrical/mechanical properties of each component. In Eq. (20), F_{tot} denotes the total vertical load and d the distance of loads from the IGU supports, while the other parameters have been previously defined. The failure load-deflection configuration was taken into account in Eq. (20) for the analytical calculations of γ.

Worth of interest, in Tables 6, 7 and 8, is the generally weak connection offered by the components in use. Such an outcome first suggests a mostly uncoupled behaviour for the involved glass panels, thus a layered distribution of stresses in each component (i.e., Fig. 4c). The second aspect that derives from the presence of weak edge connections can involve variations in load sharing effects and available simplified approaches for design (i.e., Fig. 2). Accordingly, both these aspects will be further assessed in "Part 2" with the support of numerical models.

By the moment, see Tables 6, 7 and 8, rather stable connection stiffness estimates were obtained from specimens belonging to the same series, or with rather comparable geometrical and mechanical properties. Finally, see Table 6 versus Tables 7, 8, the experimental outcomes and corresponding γ-values suggest that

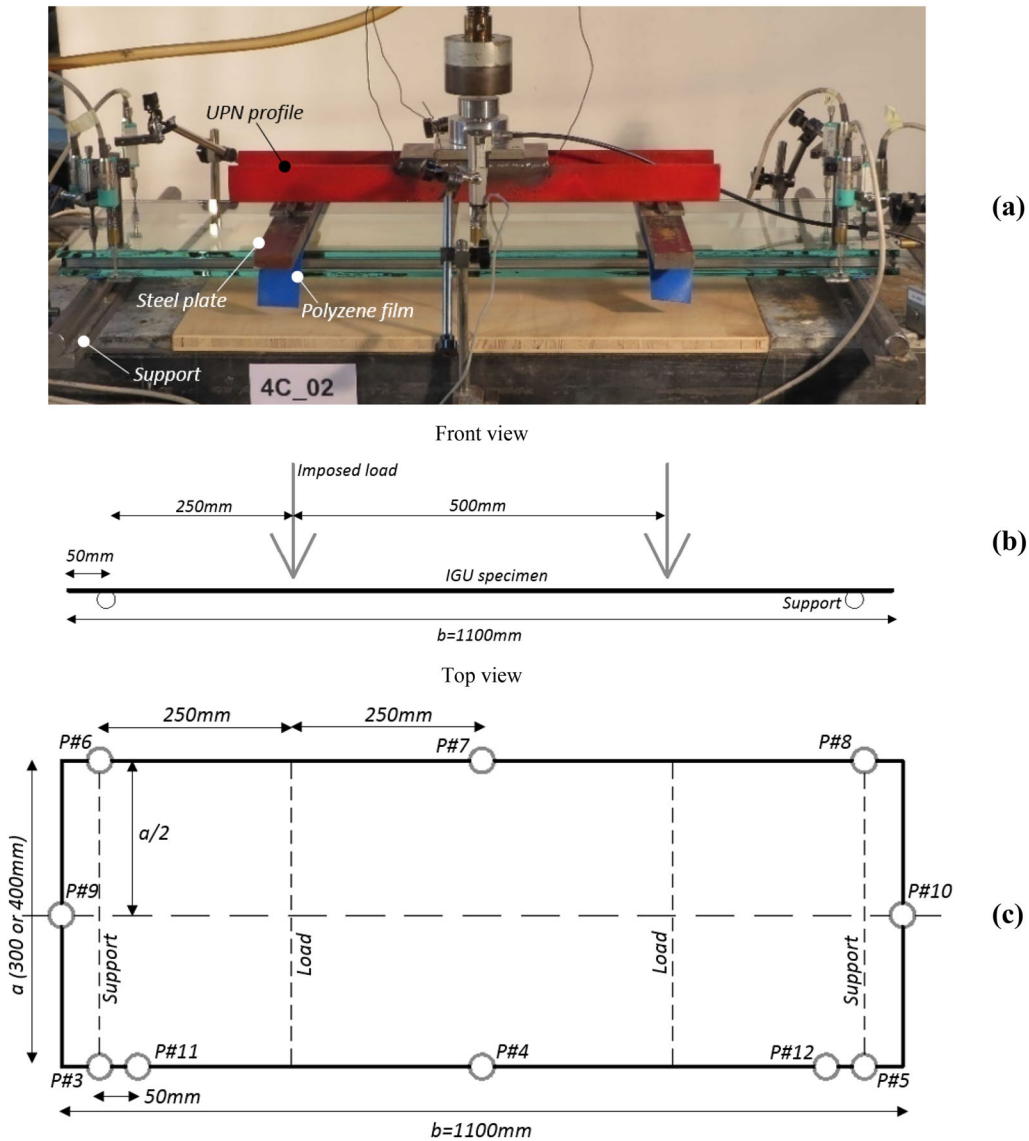

Fig. 8 Test setup for the bending experiments: **a** front view; with **b**, **c** nominal dimensions and position of instruments and **d** detail of instruments installation

(for the examined scenarios): (1) the connection efficiency is minimally affected by the WE or AL spacer bar (see Table 6); (2) the presence of silicone layers can potentially double the connection efficiency (Table 6); (3) but in the case of 4-sealed edges the effects due to the presence of silicone layers gives less pronounced γ -variations. More in detail, the progressive introduction of silicone sealed edges can be recognized by the increase of calculated γ-values.

5.3 Mechanical performance assessment and comparisons at collapse

Among the multitude of experimental records for all the tested IGU specimens (i.e., measurements from the 10 LVDTs in use), the attention was focused on some key performance parameters, namely the effects due to the presence of silicone joints, with respect to other basic systems, and the ultimate load-bearing capacity of the tested specimens.

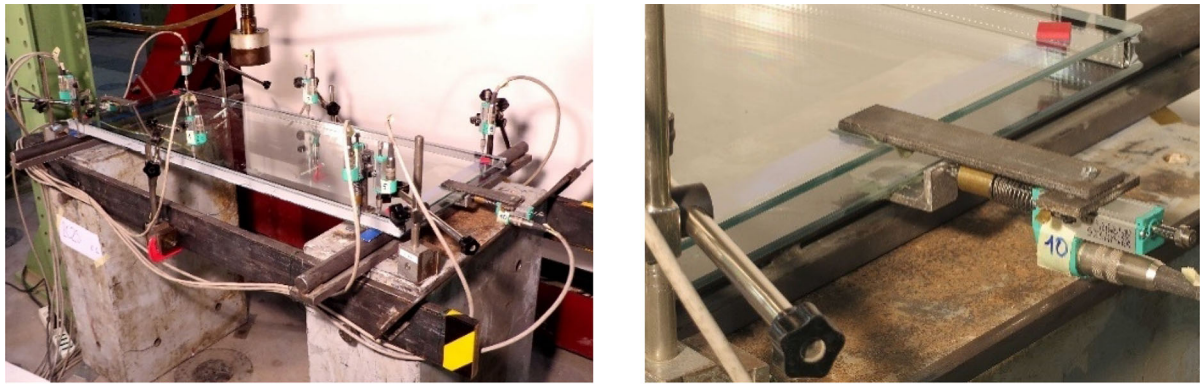

Fig. 9 Instruments for the bending experiments

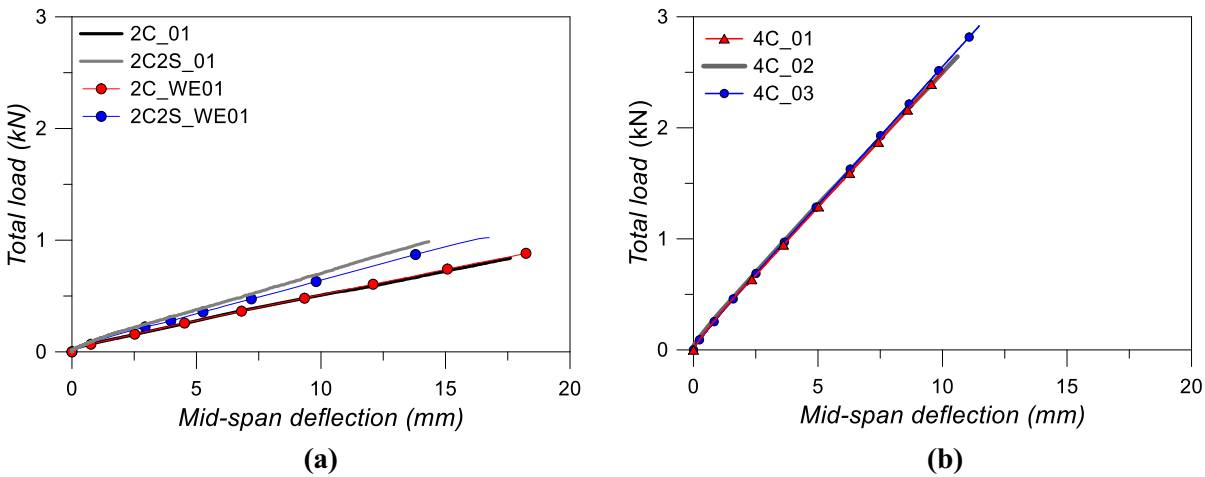

Fig. 10 Load-deflection response for selected IGUs. Examples for **a** 2-edge or **b** 4-edge sealed specimens

Besides the limited number of configurations object of analysis, for example, from Fig. 10 it can be perceived that:

- A mostly identical bending behaviour was obtained for similar specimens (with AL or WE spacer bars), see "2C_01" or "2C_WE01", both in the elastic stage and at failure. According to Table 6, both the experiments manifested a qualitatively similar cracking mechanism;
- A marked increase of bending stiffness can be noticed for the specimens with silicone joints (see "2C2S_01" and "2C2S_WE01"). For both these specimens, cracks originated from the region of load introduction.

For all the tested IGUs, load-midspan deflection curves according to Fig. 10 were collected, both for 2-edge or 4-edge sealed specimens. Major variations, due to the mechanical and geometrical features of the spacer connection in use, were observed in terms of global stiffness and ultimate load/deflection.

Given a general specimen, moreover, the presence of a partially flexible linear connection between the edges of glass panels typically resulted in:

- A certain relative sliding of glass panels in bending, both in presence of 2-side of 4-side sealed edges;
- A partial uplift of the glass panels in the region of supports, as offered by the flexibility of sealant joints, having to accommodate the global bending deformations of the glass panels as a whole;

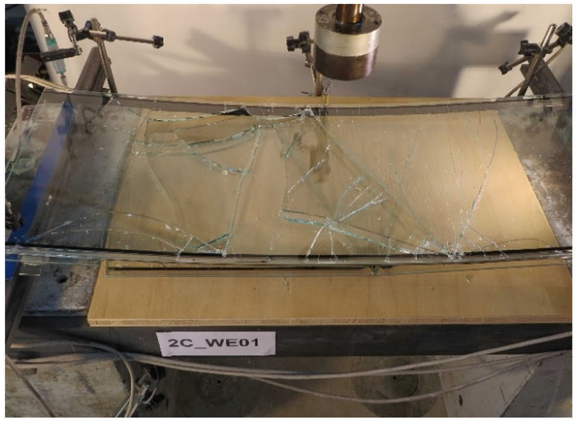

(a) 2C_WE01

(b) 2C_WE01

(c) 2C2S_WE01

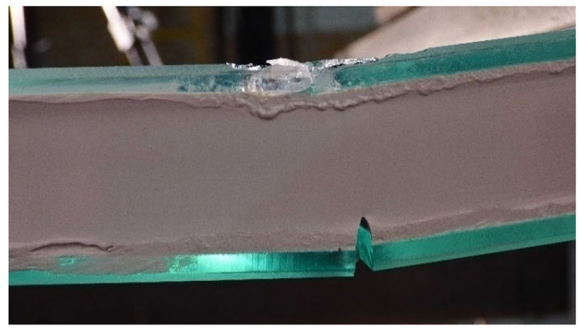

(d) 2C2S_WE01

(e) 4C_03

(f) 4C2S_03

Fig. 11 **a–f** Typical failure mechanism from bending tests on IGUs (selected specimens)

Table 6 Failure mechanism for IGUs with WE spacer bar (5 mm thick glass panels)

Specimen	Cracking type	Cracking panel	Crack origin	Connection efficiency γ
2C_01	Several distributed cracks	Bottom	Mid-span	0.031
2C_WE01	Several distributed cracks	Bottom	Mid-span	0.026
2C2S_01	Several distributed cracks	Bottom	Load introduction	0.054
2C2S_WE01	Radial pattern (single crack)	Bottom	Load introduction	0.042

Table 7 Failure mechanism for IGUs with AL spacer bar (10 mm thick glass panels)

Specimen	Cracking type	Cracking panel	Crack origin	Connection efficiency γ
4C_01	Radial pattern (single crack)	Bottom	Load introduction	0.063
4C_02	Radial pattern (single crack)	Bottom	Mid-span	0.061
4C_03	Radial pattern (single crack)	Bottom	Mid-span	0.065
4C2S_01	Mixed	Bottom	Mid-span	0.074
4C2S_02	Mixed	Bottom	Load introduction	0.074
4C2S_03	Mixed	Bottom	Load introduction	0.075
4C4S_01	Mixed	Bottom	Load introduction	0.078
4C4S_02	Radial pattern (single crack)	Bottom	Load introduction	0.082
4C4S_03	Radial pattern (single crack)	Bottom	Load introduction	0.080

Table 8 Failure mechanism for IGUs with WE spacer bar (10 mm thick glass panels)

Specimen	Cracking type	Cracking panel	Crack origin	Connection efficiency γ
4C_WE01	Several distributed cracks	N.a.	Load introduction	0.063
4C_WE03	Several distributed cracks	N.a.	Mid-span	0.065
4C2S_WE01	Radial pattern (single crack)	Bottom	Mid-span	0.078
4C2S_WE02	Radial pattern (single crack)	Bottom	Load introduction	0.083
4C2S_WE03	Several distributed cracks	N.a.	Mid-span	0.084
4C4S_WE01*	Several distributed cracks	N.a.	Load introduction	0.057
4C4S_WE02*	Several distributed cracks	N.a.	Load introduction	0.048
4C4S_WE03*	Several distributed cracks	Bottom	Mid-span	0.047
4C4S_WE01	Radial pattern (single crack)	Bottom	Mid-span	0.082
4C4S_WE02	Radial pattern (single crack)	N.a.	Load introduction	0.077
4C4S_WE03	Radial pattern (single crack)	Bottom	Load introduction	0.083

*= with 5 mm thick glass panels, $a = 400$mm

- While mostly coherent vertical deformations were measured for both the top and bottom glass panels in the mid-span section of IGU samples.

For sake of clarity, comparative test results are thus proposed in this paper in the form of a series of charts, being representative of key performance indicators for the tested IGUs, as obtained by grouping them together.

A first group of specimens with WE spacer bar and 5 mm thick glass panels was first taken into account, see Fig. 12. The experimental results of 2-edge sealed specimens of Fig. 10 are proposed in comparison to the 4C4S_WE series (3 specimens with identical features). The presence of 4-edge connections, see Fig. 12a, first manifested in enhanced performance of bonded glass panels as a whole composite system, thus in a marked increase of ultimate load for all the specimens (+ 43% the mean increase of 4-edge sealed samples, compared to 2-edge sealed specimens). For the 4-edge sealed specimens with silicone joints, the enforced mechanical interaction of glass panels can be also perceived in Fig. 12c, in the form of global bending stiffness (+ 14% the mean increase of stiffness, with respect to 2-edge sealed specimens). Beside the substantial modification of bending performances for the 2- or 4-edge sealed samples of Fig. 12, finally, no marked variations where observed in terms of relative longitudinal sliding of the top and bottom glass panels. Such an outcome can be noticed in Fig. 12d, where the mean sliding at failure was measured in the order of 1.7mm (± 3% of scatter).

A second set of comparisons was carried out by comparing the bending performances of 4-sealed edges and WE spacer, see Fig. 13. Compared to the first group of specimens in Fig. 12, the key variation was represented by the thickness of glass panels (10 mm thick in place

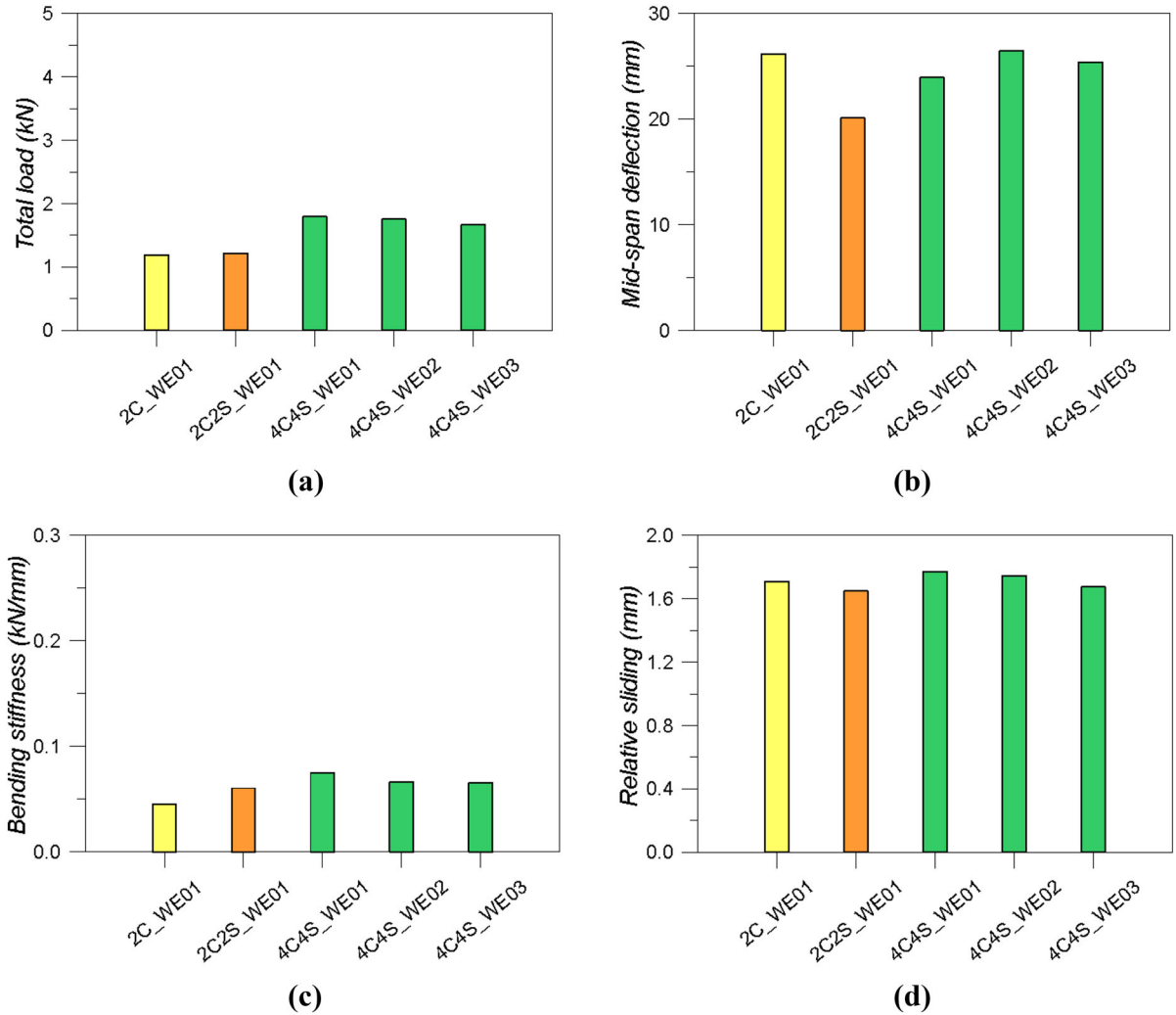

Fig. 12 Bending response at collapse for selected IGU specimens with WE spacer bar and different seals (5 mm thick glass panels): **a** ultimate load; **b** ultimate deflection at mid-span, with **c** bending stiffness and **d** relative longitudinal sliding of glass panels

of 5 mm), thus corresponding to an increased glass-to-IGU bending stiffness ratio. Moreover, the sensitivity of specimens performance to the presence of silicone joints along 2 (longest) edges or 4 edges was primarily taken into account.

In Fig. 13a, b, experimental comparisons are hence proposed in terms of total load at failure for the bending tests and corresponding global stiffness, for three series of specimens. Two samples (4C_WE01 and 4C_WE03) are without silicone joints, while three others are inclusive of the secondary seals along 2 edges ("4C2S_WE" series). Finally, the "4C4S_WE" series includes silicone joints for all the 4 edges. Besides such a major variation in the specimens features, see Fig. 13a, the experiments showed no marked increase in terms of ultimate load at failure for them. Starting from the "4C_WE" series (3.6 kN the mean ultimate load), the inclusion of silicone along 2 or 4 edges resulted respectively in load increases up to + 1.6% and 7.1%.

A certain scatter, however, was also perceived among the three specimens belonging to each series. The latter was estimated in ± 4% and ± 7% for 2- or 4-edge silicone joints, with respect to the mean ultimate load. This effect is partly in contrast with Fig. 12a, with ± 3% the mean load variation for the "4C4S_WE" series, but could be rationally justified by the presence

of stiffer glass panels (10 mm in thickness), with identical flexible connections. Accordingly, the presence of silicone joints along 2 long edges only (or 4 edges respectively) and stiff panels proved to minimize the possible structural benefits due to the presence of a load-bearing bonding layer along the glass edges, especially in terms of ultimate load carried out by the tested specimens. Another influencing parameter that should be further assessed with the support of FE simulations, however, is also represented by the possible scatter in the tensile strength of glass, hence possibly affecting the bending performance estimates at failure.

A certain progressive benefit due to the presence of silicone joints was indeed observed by taking into account the global bending stiffness estimates for the same series of tests, see Fig. 13b. In the latter case, silicone layers proved to increase up to + 16.5% the global stiffness for all the "4C_WE" specimens. Also in this case, however, a certain misleading effect was noticed by comparing the group of specimens as a whole. For the "4C4S_WE" series, for example, the average bending stiffness was found to partly decrease, with respect to the specimens with 2 silicone bonds.

Such a variation was calculated in −0.88% scatter, that even small, is counterintuitive. Possible manufacturing defects could justify such an experimental observation.

A marked increase of bending stiffness was in any case observed for all the specimens with silicone joints in Fig. 13b, with respect to the "4C" specimens (with + 13.8% the mean stiffness increase for combined "4C2S_WE" and "4C4S_WE" samples), thus enforcing the beneficial contribution of silicone bonds.

One last consideration was spent for selected specimens of Figs. 12 and 13, and more in detail the "4C4S_WE" series that were investigated with both 5 mm ($a = 400\,\text{mm} \times b = 1100\,\text{mm}$) or 10 mm thick glass panels ($a = 300\,\text{mm} \times b = 1100\,\text{mm}$). Assuming a double factor for the thickness of glass (and given also the variation in the width a), an ideal bending stiffness variation up to 6 would be expected (beam-like behaviour assumption). From the experiments, however, the latter was calculated in ≈ 4.5 times (+ 331%) for IGUs with 10 mm thick glass. Doubling the glass thickness, moreover, was found to result in a more than double ultimate load (+ 121% the mean increase), while a + 38% longitudinal sliding was calculated for the 10 mm thick panels (i.e., ≈ 1.05mm), compared to the 5 mm thick specimens.

A third group of specimens was assessed, with careful consideration for IGUs with 10 mm thick glass panels and AL spacer bar, see Fig. 14.

There, the experimental results are proposed for three series of specimens, each one including three samples with identical nominal geometry and mechanical properties. According to Fig. 13, the experimental comparisons proposed in Fig. 14 were obtained by taking into account few key variations in the 4-edge sealed samples, that is:

- The presence of AL bars with Butylver seal only ("4C" series);
- The presence of AL bars with Butylver seal, plus 2-long edges sealed by silicone joints ("4C2S" series);
- And finally the presence of AL bars with Butylver seal and silicone joints for all the 4 edges ("4C4S" series).

As far as the experimental results are proposed in the same order for the selected series (i.e., "4C", "4C2S" and "4C4S"), it is possible to notice in Fig. 14a that the ultimate load progressively increases, as far as the flexible linear connection along the edges is improved by the addition of silicone joints. Globally, the load increase was calculated in + 19% and + 23% respectively for the "4C2S" and "4C4S" series, with respect to the "4C" basic group of samples.

For each series with silicone joints, the scatter from mean ultimate load estimates was predicted in ± 3% and ± 4% for the "4C2S" and "4C4S" groups respectively.

Accordingly, a certain increase of bending stiffness was also measured when progressively introducing the silicone joints along the edges, see Fig. 14b. Such a bending stiffness variation, compared to the "4C" series of specimens, was calculated in + 9.5% and + 15% respectively, for the specimens with silicone joints along 2 or 4 edges. Even more stable estimates were also noticed for specimens belonging to the same series. Stiffness variations in the range of ± 1.6%, ± 0.4% and ± 1.5% were calculated for "4C", "4C2S" and "4C4S" groups.

In conclusion, a final attempt was finally carried out to assess possible variations due to the use of AL or WE spacer bars, with 4-edge sealed specimens with identical sealants and glass thickness (10 mm). Compared to WE specimens of Fig. 13, for example, the AL specimens in Fig. 14 proved to offer a more stable bending

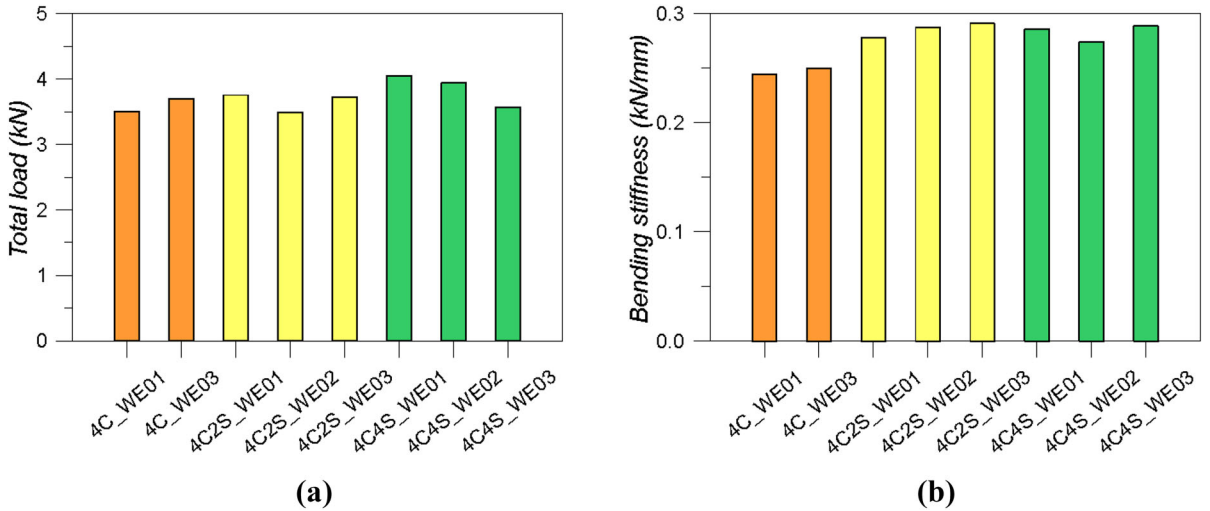

Fig. 13 Bending response at collapse for selected IGU specimens with WE spacer bar and different seals (10 mm thick glass panels): **a** ultimate load, **b** bending stiffness (*note*: 4C_WE02 results are omitted due to techcnical troubles with instruments)

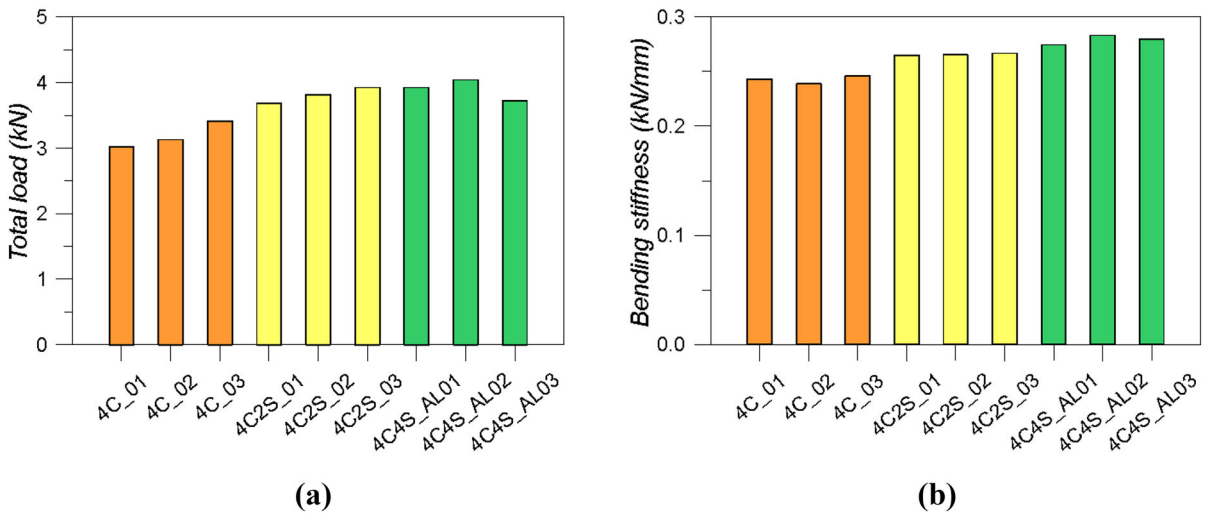

Fig. 14 Bending response at collapse for selected IGU specimens with AL spacer bar and different seals (10 mm thick glass panels): **a** ultimate load, **b** bending stiffness

behaviour, with limited variations for the pre-cracked load-deflection of specimens with similar properties. As far as mean test results are taken into account for series of samples, the ultimate load carried out by the AL specimens was calculated in the order of + 4% the corresponding WE specimens.

The global bending stiffness of AL specimens with silicone joints, on the other hand, was found to be smaller than WE samples (up to − 6.9%, for 2-silicone edges), thus suggesting the need of a more detailed analysis of local and global mechanical behaviours for the specimens object of analysis.

5.4 Mechanical performance assessment and comparisons at intermediate load levels

At a final stage of the experimental investigation, the sensitivity of bending stiffness estimates was carried out by taking into account different load levels (in the

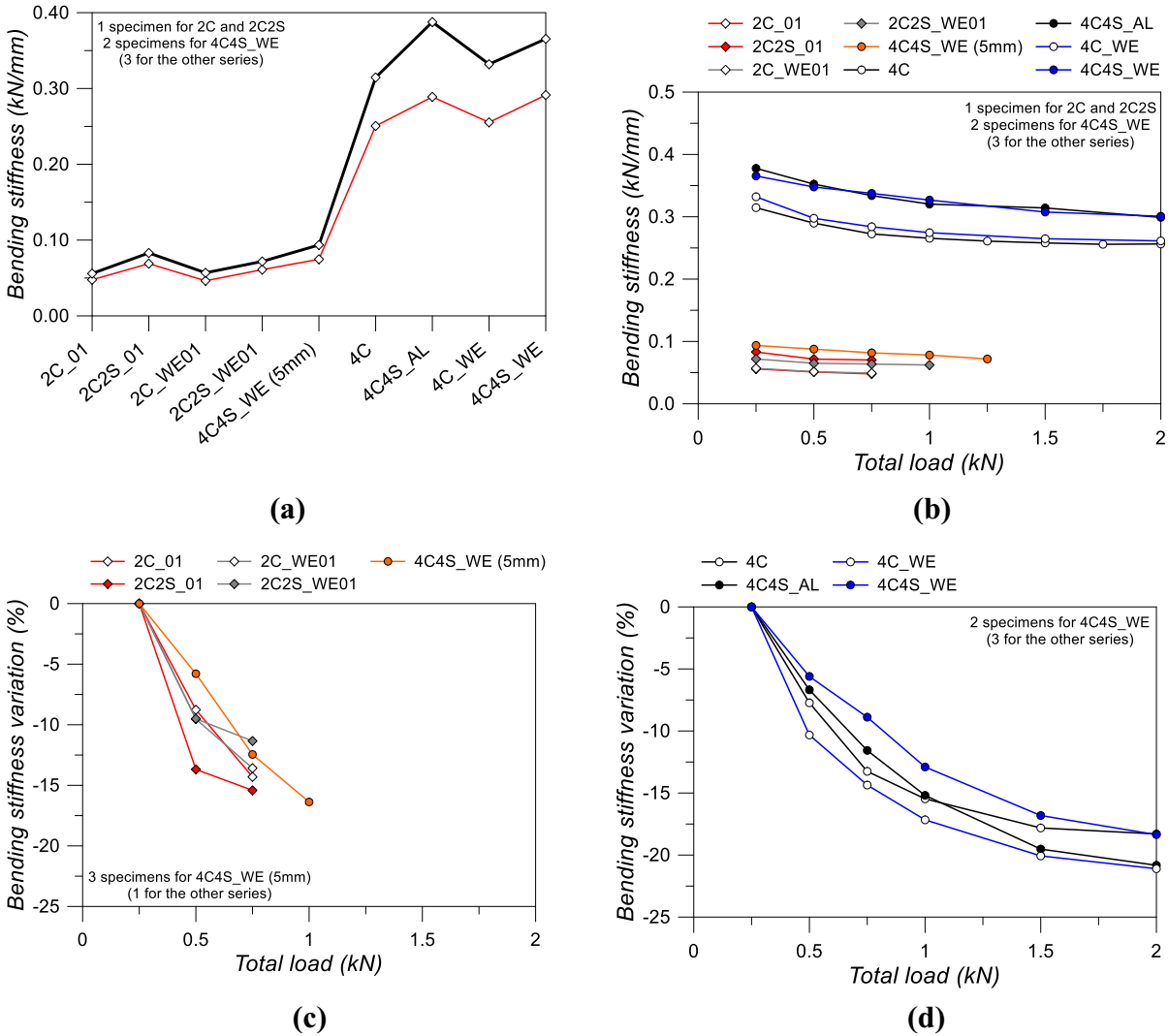

Fig. 15 Bending stiffness variation at different load levels, for selected IGU specimens: **a** stiffness estimates for 0.25 kN and collapse conditions, with **b** stiffness variation as a function of the imposed load, and **c**, **d** stiffness percentage variations

range of 0.25–2 kN of total load), for all the specimens herein discussed.

As already emphasized in Sect. 5.3, the "2C" and "2C2S" series results were thus regarded as single specimens. The "4C" and "4C4S" results, otherwise, were defined as the average calculation for each series. Figure 15, in this regard, shows the experimentally obtained bending stiffness estimates for the most relevant configurations. Figure 15a, in particular, clearly emphasizes a certain stiffness variation for the tested specimens, as a function of the imposed load. The effect of both the glass thickness (5 mm or 10 mm), as well as the presence of silicone layers can be clearly perceived in Fig. 15b, at a given loading stage. A more detailed analysis of results was thus carried out by taking into account the percentage variation of stiffness for the same specimens, with respect to an initial value (0.25kN), see Fig. 15b, c.

For the 2-edge sealed specimens, for example, Fig. 15c shows that the stiffness variation is less pronounced when the silicone layers are present. At the same time, the 4C4S specimens with 5 mm thick glass panels are even less sensitive to the progressive degradation of sealants in use. For the 4-edge sealed speci-

mens with 10 mm glass panes (Fig. 15b), a more than double stiffness increase was found, as also partly emphasized in Sect. 5.3. Worth of interest, however, is that the calculated stiffness variations were found to be mostly in line for 5 mm and 10 mm thick glass specimens, under different load levels (Fig. 15c, d). The global stiffness decrease at failure, finally, was generally detected in the range of -15% up to -24%, for the 2-edge and 4-edge sealed specimens respectively.

6 Conclusions

Insulated glass units (IGUs) are largely used in buildings, due to a series of motivations. Among others, IGUs can be involved as mechanical systems able to behave as composite assemblies characterized by the presence of linear connections along their edges. As such, dedicated methods of analysis and design are conventionally required to capture their actual mechanical performance, first of all the well-known load sharing effects.

In this paper, careful consideration was spent for the experimental analysis of IGUs characterized by the presence of different spacer connections and sealants. A focus was in fact dedicated to the use of different spacer bars (aluminium or warm edge), but also to the presence of primary and secondary seals (in this study, butyl and silicone layers). An extended experimental program inclusive of shear tests on small-scale IGU triplets and four-point bending tests on IGU specimens was hence carried out. Based on the experimental observations and measurement, the effect of spacer connection details was preliminary assessed, towards the definition of relevant mechanical parameters of interest for practical design considerations and reliable FE numerical calculations. Among others, a first attempt was spent for the analysis of shear mechanical properties for typical spacer connections (i.e., ultimate resistance, ultimate/serviceability stiffness and ultimate shear stress/deformation). As a major outcome of the preliminary experimental study, for example, it was shown that the IGU specimens in shear typically manifested a ductile failure mechanism, due to the activation of silicone bonding layers, in combination with rigid-body deformations of the involved bars. On the other side, pure shear loads do not reflect the actual loading performance for IGU connections.

Accordingly, four-point bending tests were proposed for IGUs with various features. The silicone layers, as shown, proved to significantly increase the global mechanical performances for a given IGU geometry in bending. Throughout the series of bending tests, relevant modifications of ultimate load predictions and global bending stiffness estimates where observed thanks to the analysis of 2-edge or 4-edge sealed specimens (with/without the silicone layers). The experimental observations for the selected geometrical configurations highlighted, in particular, that silicone layers can efficiently improve the load-bearing performance of a given IGU, with up to $+23\%$ of ultimate load and $+15\%$ bending stiffness estimates (AL spacer bar). A less pronounced performance improvement at collapse was obtained for WE specimens, with $+7\%$ and 16.5% the ultimate load and stiffness variations in presence of silicone bonds. Besides that, the experimental measurements also proved that the typical linear spacer connections are mostly representative of weak continuous restraints for glass edges, thus corresponding to mostly independent, layered mechanical performance of the involved panels.

Another relevant aspect was then represented by the typical failure mechanism that was experimentally observed. Given that all the bending specimens manifested a brittle collapse mechanism governed by fracture of glass panels (and progressive debonding of sealant layers), the presence of silicone layers was often associated to a substantial modification of the observed cracks (i.e., origin and distribution), due to the additional flexibility of edge connections.

Finally, the experimental study emphasized a progressive stiffness degradation for all the tested specimens, as a function of increasing imposed loads. Worth of interest, in this case, is the effect of spacer connection features and progressive damage on the typical load sharing phenomena, and such an aspect will be further explored ("Part 2").

Certainly, such a kind of experimental outcomes is strictly related to the key properties of the tested specimens (small-scale prototypes composed of monolithic glass panels). Several other aspects that can have a relevant role in the load-bearing performance of IGUs should be properly taken into account. Accordingly, the experimental investigation herein reported will be further explored with the support of analytical and FE numerical models, aiming at an appropriate quantifica-

tion of the response and sensitivity of full-scale IGUs to the spacer connection features.

Acknowledgements Ing. Pasquale Lucia (BLDing Studio, www.blding.it) and Zanatta Vetro S.p.A. (www.zanattavetro.it) are acknowledged for providing the IGU specimens. A special thanks for Ing. Franco Trevisan (University of Trieste), for the technical support during the whole experimental investigation. Finally, Ing. Irene Panizzut is acknowledged for her collaboration.

Compliance with ethical standards

Conflict of interest The authors declare that they have no conflict of interest.

References

Bedon, C., Amadio, C.: A linear formulation for the ULS design of glass elements under combined loads: application to IGUs. Glass Struct. Eng. **3**(2), 289–301 (2018a)

Bedon, C., Amadio, C.: Buckling analysis and design proposal for 2-side supported double insulated glass units (IGUs) in compression. Eng. Struct. **168**, 23–34 (2018b)

Bedon, C., Amadio, C.: Mechanical analysis and characterization of IGUs with different silicone sealed spacer connections—part 2: modelling. Glass Struct. Eng. (2020). https://doi.org/10.1007/s40940-020-00123-9

EN 485–2: Aluminium and aluminium alloys—sheet, strip and plate—part 2: mechanical properties. CEN—European Committee for Standardization, Brussels, Belgium (2016)

EN 572–2: Glass in buildings—basic soda lime silicate glass products. CEN—European Committee for Standardization, Brussels, Belgium (2004)

EN 573–3: Aluminium and aluminium alloys—chemical composition and form of wrought products—part 3: Chemical composition and form of products. CEN—European Committee for Standardization, Brussels, Belgium (2019)

EN 1995-1-1. Eurocode 5: design of timber structures. CEN—European Committee for Standardization, Brussels, Belgium

EN 10088–2: Stainless steels—part 2: technical delivery conditions for sheet/plate and strip of corrosion resisting steels for general purposes. CEN—European Committee for Standardization, Brussels, Belgium (2014)

Feldmann, M., Ungermann, D., Abeln, B., Baitinger, M., Preckwinkel, E., et al.: Development of innovative steel-glass-structures in respect to structural and architectural design (INNOGLAST). RFCS Research Project No (2010). RFCS-CT-2007-00036

Feldmann, M., Kasper, R., Abeln, B., Cruz, P., Belis, J., Beyer, J., et al.: Guidance for European structural design of glass components—support to the implementation, harmonization and further development of the Eurocodes. Report EUR 26439, Joint Research Centre-Institute for the Protection and Security of the Citizen. https://doi.org/10.2788/5523, Pinto Dimova, Denton Feldmann (Eds.) (2014)

Firmo, F., Jordão, S., Costa Neves, L., Bedon, C.: The effect of adhesive joints on the performance of hybrid steel-glass beams—an analytical and experimental study. In: Challenging Glass Conference Proceedings, vol. 5, pp. 171–186, ISSN 2589-8019 (2016)

McMahon, S., Norville, H.S., Morse, S.M.: Experimental investigation of load sharing in insulating glass units. J. Arch. Eng. **24**(1), 04017038 (2018)

Möhler, K.: Über das Verhalten von Biegeträgern und Druckstäben mit zusammengesetzten Querschnitten und nachgiebigen Verbindungsmitte, TH Karlsruhe (1956)

Morse, S.M., Norville, H.S.: Comparison of methods to determine load sharing of insulating glass units for environmental loads. Glass Struct. Eng. **1**(1), 315–329 (2016)

Nguyen-Tri, P., Triki, E., Nguyen, T.A.: Butyl rubber-based composite: thermal degradation and prediction of service lifetime. J. Compos. Sci. **3**, 48 (2019). https://doi.org/10.3390/jcs3020048

Pascual, C., Montali, J., Overend, M.: Adhesively-bonded GFRP-glass sandwich components for structurally efficient glazing applications. Compos. Struct. **160**, 560–573 (2019)

prEN 13474–1: Glass in building—design of glass panes—part 1: general basis of design. CEN—European Committee for Standardization, Brussels, Belgium (2007)

Starman, B., Macek, A., Rus, P., Obid, S., Kralj, A., Halilovic, M.: Primary seal deformation in multipane glazing units. Appl. Sci. **10**, 1390 (2020). https://doi.org/10.3390/app10041390

Turowec, B.A., Gillies, E.R.: Synthesis, properties and degradation of polyisobutylene-polyester graft copolymers. Polym. Int. **66**(1), 42–51 (2016)

Van Den Bergh, S., Hart, R., Jelle, B.P., Gustavsen, A.: Window spacers and edge seals in insulating glass units: a state-of-the-art review and future perspectives. Energy Build. **58**, 263–280 (2013)